Journal of Applied Fluid Mechanics, Vol. 9, No. 4, pp. 1791-1798, 2016.
Available online at www.jafmonline.net, ISSN 1735-3572, EISSN 1735-3645.
DOI: 10.18869/acadpub.jafm.68.235.24206

Study of Flow Patterns in Radial and Back Swept Turbine Rotor under Design and Off-Design Conditions

S. P. Shah[1†], S. A.Channiwala[2], D. B. Kulshreshtha[1] and G. Chaudhari[1]

[1] *C. K. Pithawalla College of Engineering and Technology, Surat, Gujarat, 395007, India.*
[2] *S.V. National Institute of Technology, Surat, Gujarat, 395007, India*

†*Corresponding Author Email: samip_mech@yahoo.com*

(Received November 10, 2014; accepted September 30, 2015)

ABSTRACT

Paper details the numerical investigation of flow patterns in a conventional radial turbine compared with a back swept design for same application. The blade geometry of a designed turbine from a 25kW micro gas turbine was used as a baseline. A back swept blade was subsequently designed for the rotor, which departed from the conventional radial inlet blade angle to incorporate up to 25° inlet blade angle. A comparative numerical analysis between the two geometries is presented. While operating at lower than optimum velocity ratios (U/C), the 25° back swept blade offers significant increases in efficiency. In turbocharger since the turbine typically experiences lower than optimum velocity ratios, this improvement in the efficiency at off-design condition could significantly improve turbocharger performance. The numerical predictions show off-design performance gains of the order of 4.61% can be achieved, while maintaining design point efficiency.

Keywords: Gas turbine impeller; Numerical simulation.

1. INTRODUCTION

The turbocharger turbine rotor will experience a high value of positive incidence during off-design condition, where the turbine is operating at low U/C values, in the range of 0.3 to 0.5, resulting poor blading, high blade loading, tip leakage and separation on suction surface. These secondary flow structures propagate down the blade passage causing an increase in entropy and hence reduction in efficiency. The flow structure in the blading on design condition was studied by number of authors but few have looked at the effects of operating at low U/C values. Meitner and Glassman (1983) adopted an existing computer program to allow the inclusion of back swept blading. The analysis was carried out on two rotors, one with 15° back swept and other with 30°. The program predicted a more efficient rotor at off-design conditions and this was attributed to better flow alignment at inlet. The 1D work carried out by Hakeem (1995) shows that the optimum velocity ratio could be defined as a function of inlet blade and inlet flow angle. A number of different blade geometry were tested by Mully and Weber (2001) in order to improve off-design efficiency for automotive turbocharger application and found that at low rotational speed, the rotor with back swept curved blade aligned better with the flow and reduces the magnitude of exit swirl. The detail numerical and experimental analysis was more recently carried out by Barr *et al*. (2008) to check effect of implementing back swept blading at inlet region of a radial turbine. Stress levels in the turbine blade were also carried out to assess the impact of such design by FEA. The analysis suggested that back swept blade has better ability to deal with high positive incidence at low velocity ratio and hence leading to low flow separation on blade suction side. Palfreyman *et al*. (2002) compared the benefits offered from a mixed flow turbine over the radial turbine. Due to the mixed flow turbine having a smaller radius at the hub, flow turns into the passage. At the leading edge, due to the blade loading characteristics, tip flow leakage dominated the full length of the blade pitch at the shroud. It was also noted that the Coriolis force had a strong influence on the blade loading at inlet. Furthermore, as the flow turned from the radial to axial direction, separation occurred just at the shroud near the leading edge tip of the radial flow turbine. This flow interacted with the tip leakage to generate another vortex which grew as it propagated downstream.

This paper looks at the flow development within radial and back swept rotor. A 25kW turbine was first designed and used as a base line model and then back swept blade was subsequently designed

for the rotor, which departed from the conventional radial inlet blade angle up to 25° inlet blade angle. Initially one-dimensional investigation was carried out on radial and back swept blade to investigate gain in efficiency when operating at lower velocity ratio and then the results are compared with 3D numerical simulation. The 3-D analysis is then extended to examine internal flow fields in order to understand the features that contribute towards the change in turbine efficiency.

2. ONE-DIMENSIONAL PERFORMANCE PREDICTION

One-dimensional performance predictions for both the baseline rotor and the 25° backswept rotor were assessed using AxSTREAM turbomachinery design software to obtained potential gain in efficiency offered by back swept bleading. In order to asses potential gain in efficiency offered by back swept blading. The 1D modeling procedure was based on method described by G. Stepanov's and corrected Craig & Cox's. The same loss models used to maintain consistency for each of geometry analyzed. Here, back swept inlet angle as the angle measured from the radial direction opposite the direction of blade rotation (J. Walkingshaw *et al*. 2011), as shown in Fig. 1. The dimension of designed turbine for 25 kW power at maridional plane are shown in Fig. 2.

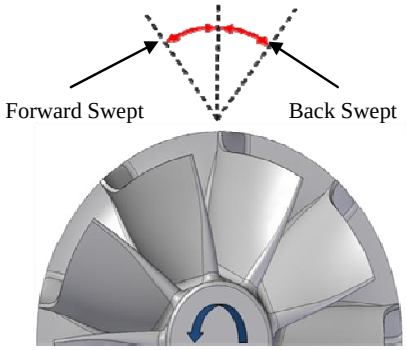

Fig. 1. Naming Convention used for Inlet Blade Angle Study.

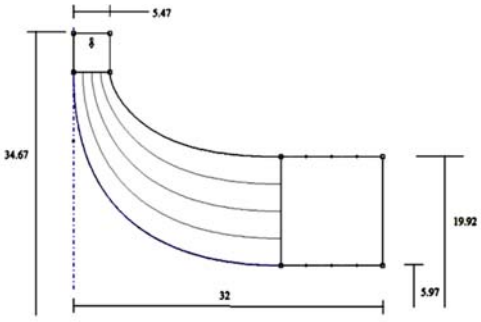

Fig. 2. Turbine Dimension in Maridional Plane.

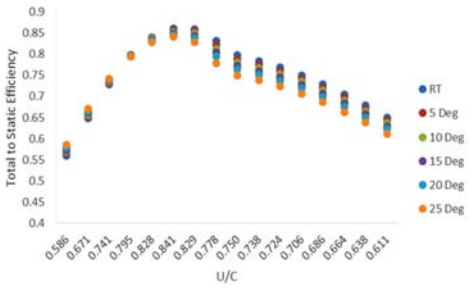

(a) Total to Static Efficiency vs. Velocity Ratio (Inlet Pressure 1.8)

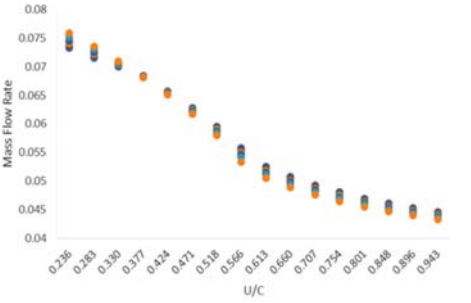

(b) Mass Flow rate vs. Velocity ratio (Inlet Pressure 1.8)

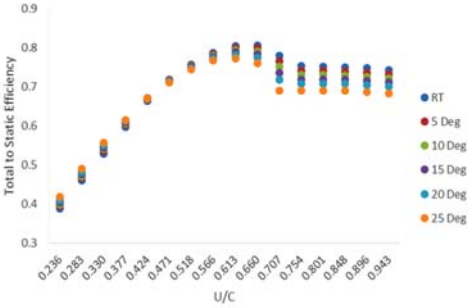

(c) Total to Static Efficiency vs. Velocity Ratio (Inlet Pressure 2.8)

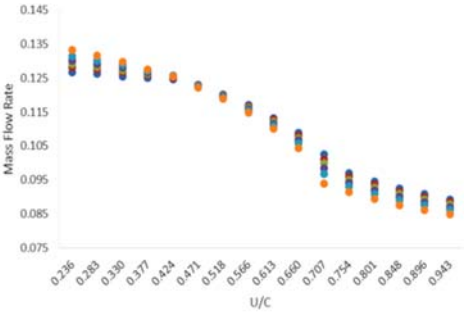

(d) Mass Flow rate vs. Velocity ratio (Inlet Pressure 2.8)

Fig. 3. One Dimensional Predictions.

For the baseline radial rotor and the 25^0 back swept rotors, Fig. 3 details 1D predicted efficiencies and mass flow rates plotted against velocity ratio U/C respectively. The predictions are plotted at a constant inlet pressure of 1.8 bar and 2.8 bar by keeping outlet constant pressure as 1.1 bar. It is clear from Fig. 3(a) and 3(c) that at lower than optimum velocity ratios (0.707), the

25^0 back swept rotor offers significant increases in efficiency. Back swept rotor of 25^0 offers an increase in efficiency of 3.32% over the baseline radial rotor for 1.8 bar inlet pressure at approximately 40% of the design speed (U/C = 0.235). At 2.8 bar inlet pressure efficiency increase up to 8.19%, at 40% of the design speed. As seen in Fig. 3 (b) and 3(d) an increase in mass flow through rotor. This is because of reduction in losses offered from 25° back swept rotor. This is because of better blade alignment with the more tangential flow at inlet experienced at low speeds. This improvement in performance is visualized up to a velocity ratio of approximately 0.471. After that the efficiency level of 25° back swept rotor is seen to drop below that of the baseline radial rotor. At the velocity ratio 0.707 (design point) the efficiency of the 25° back swept rotor drops 1.158% below the predicted efficiency of the baseline radial rotor. The 1D analysis predicts that 25° back swept rotor has 2.27% loss in peak efficiency relative to its radial counterpart, while offering generous advantages at lower than optimum velocity ratios.

3. DEVELOPMENT OF NUMERICAL MODEL

The real flow structures within rotor passage could not account by 1D analysis so, 3D numerical investigation was carried out using ANSYS-CFX software. A single passage model was used with periodic interface to account the domain motion. The rotor- shroud clearance was considered as 5% of the rotor blade height. Total pressure at inlet and static pressure at outlet were defined as a boundary condition. Heat transfer from the turbine was assumed to be negligible, mainly due to the insulation of the turbine case, and therefore the walls were going to be considered as adiabatic.

A variety of papers can be found in the literature dealing with the different viscous models for turbomachinery simulations. It was found in literature that, in most turbomachinery applications, the SST model has been applied over a wide range of validations cases (F.R. Menter *et al*. 2003) Menter *et al*. (2004) applied the SST model for turbomachinery simulations, showing a good agreement between the computations and the experimental data for all the cases considered. These cases showed the ability of the model to capture the effects of the variations of Reynolds number and flow separation in a wide range of conditions. The SST model is used to perform CFD simulations in an axial fan by K. S. Lee *et al*. (2008). Other application of the SST model in turbomachinery simulations is found in (R. Pecnik *et al*. 2011) in which the uncertainty of transition prediction is analyzed. Simpson *et al*. (2009) used the SST in CFD simulations of a vanned and a vaneless radial turbine showing good results. In view of the results found in the literature in which the SST model has been proved to provide valid results, this model is used for the computations performed in this work.

3.1 Mesh Independence

The 3D meshes used for the computations were shown in Fig. 4.

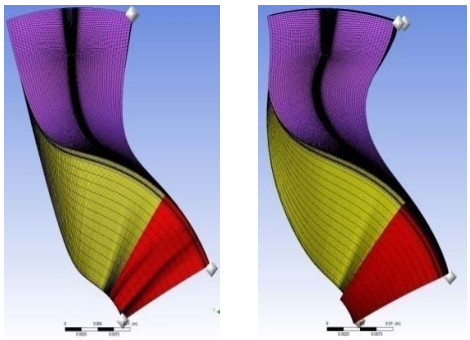

(a) Radial Turbine Mesh (b) 25^0 Back Swept Turbine Mesh

Fig. 4. Structure Mesh.

The main difficulty when dealing with real geometries is the achievement of an appropriate mesh. In this work a conformal mesh is used. The mesh has been built using I/J/C/L-grid (Traditional with control points) method. Ansys Turbogrid offers the possibility of generating a structure grid using the algorithm described in Ansys Inc. user's guide (2009). The main advantage of using a structure grid is that they have better accuracy than the equivalent tetrahedral one or, in other words, is possible to achieve the same resolution with a reduced number of cells. On the one hand, if the cell refinement is not properly done, it may cause an increase of cells aspect ratio, and the use of distorted cells can introduce convergence errors and even spurious solutions. Although the SST turbulence model was chosen, and its automatic wall treatment (R. Pecnik *et al*. 2011) has the advantage of ensuring as high degree of grid independence is possible, it is necessary to evaluate that the value of y+ is in the range of application of the wall-function (Ansys Inc. user's guide 2009). The y+ is a function of the mesh size, its definition can be found in the book of Versteeg and Malalasekera (2007).For the present case y+ values of less than 4 was achieved in most of the areas and convergence criteria of 1e-04 for residual values was imposed.

In order to study the mesh refinement the mass flow through elements needs to be studied. The rotor section is, due to its shape, the part of the original geometry where the effects of working with real digitalized geometries are more noticeable as shown in Fig. 4. This may be seen in the different fillet radius in the radial rotor and back swept rotor blades. Therefore, the structure mesh is appropriate for the rotor regions. A size function was used to increase the resolution closer to the walls. Therefore, the total number of elements is defined with the 22 block split elements. The results obtained for the rotor mesh independence in terms of mass flow rate through the rotor is shown in Fig 5.

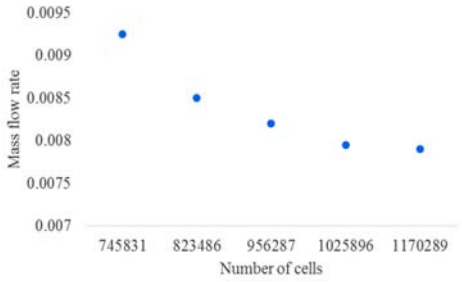

(a)The radial rotor section

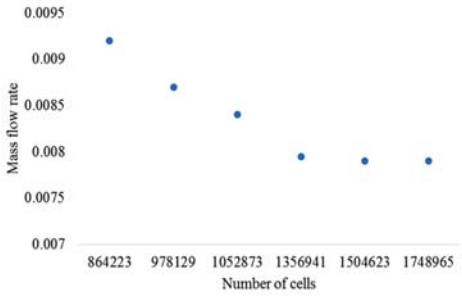

(b)The back swept rotor

Fig. 5. Mesh Independence Analysis.

3.2 CFD Results of Internal Flow Field

In order to understand the flow features that contribute to the increase in performance of the back swept rotor at low U/C values, it is necessary to study the complex 3D internal flow patterns within a rotor blade passage. 9 equispaced span wise planes between the hub and shroud were used to capture primary flow feature and 9 equispaced streamwise planes between the leading and trailing edges were used to capture secondary flow feature.

Various spanwise planes located between the hub and shroud of the baseline radial rotor and the 25° back swept rotors to express detail streamline distribution plots of the primary flow features at a velocity ratio of 0.2828 are shown infigs.6(a) to (i). Strong positive incidence is present at rotor inlet, as expected at this off-design condition. Near the hub, the relative flow pattern on the pressure side of each rotor is seen to be very similar and unable to survive with the high degree of positive incidence at inlet. A zone of recirculation is generated just downstream of the leading edge on the suction side of the blade because of flow is effectively stumble by the radially fibered leading edge causing separation. This zone of recirculation, acting as a blockage, reduces the effective flow area at inlet to the radial rotor. The 25° back swept blade is better able to adjust with the strong positive incidence at inlet, while experiencing a small amount of flow reversal. The flow is seen to follow the blade profile much better, greatly reducing the zone of recirculation, as detailed in Fig.6 (a).

Now, at 12.5% span, zone of recirculation occupies more of blade passage and covers grater potion of inlet blade region and larger in size as shown in Fig. 6(b). Here an angle of incidence increased due to viscous effect. The blockage on the suction side at inlet to the radial rotor has increased.

Just downstream of leading edge, a small zone of recirculation has developed on the suction side of the 25° back swept rotor. The development of the zone of is much more limited in 25° back swept rotor compared to radial rotor as the flow at inlet to 25° rotor not having to displace (turn) before entering blade passage. This is shown in Fig. 6 (b).

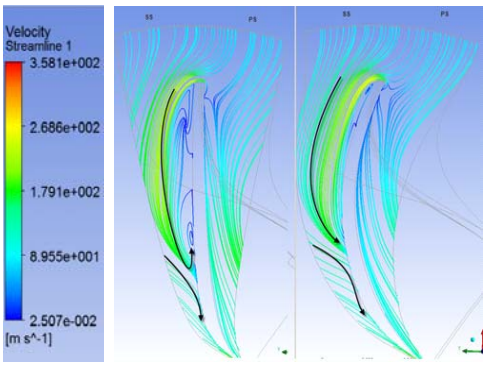

Legend Baseline Radial Rotor 25^0 Back Swept Rotor

(a) Streamline Distribution at Hub

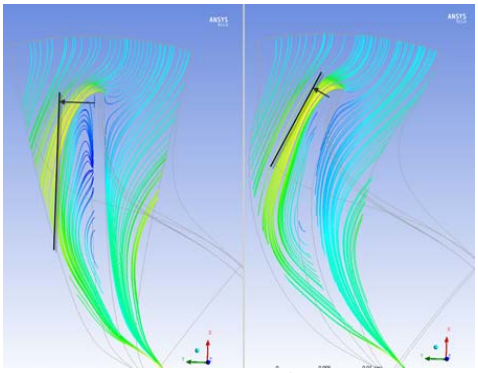

Baseline Radial Rotor 25^0 Back Swept Rotor

(b) Streamline Distribution at 12.5% Span

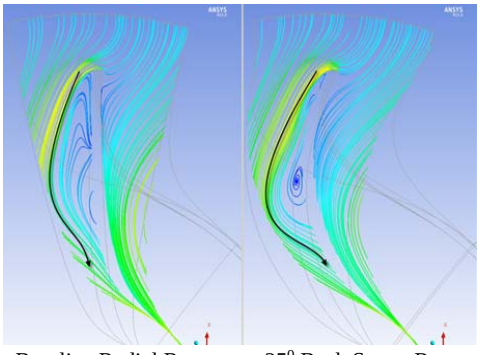

Baseline Radial Rotor 25^0 Back Swept Rotor

(c) Streamline Distribution at 25% Span

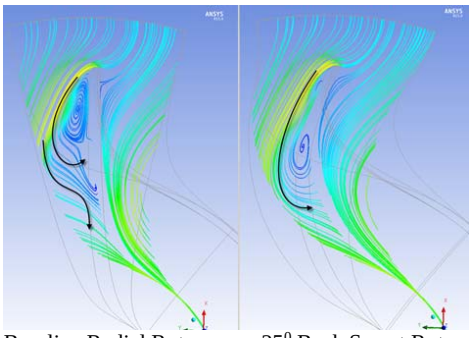

Baseline Radial Rotor 25^0 Back Swept Rotor

(d) Streamline Distribution at 37.5% Span

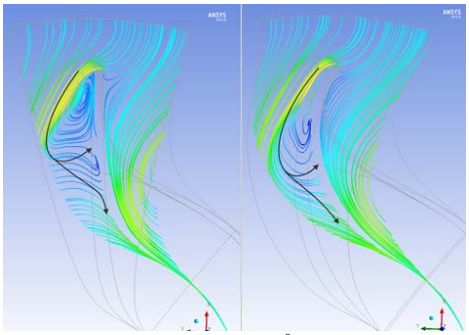

Baseline Radial Rotor 25^0 Back Swept Rotor

(e) Streamline Distribution at 50% Span

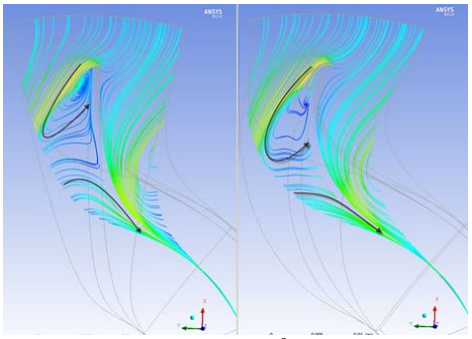

Baseline Radial Rotor 25^0 Back Swept Rotor

(f) Streamline Distribution at 62.5% Span

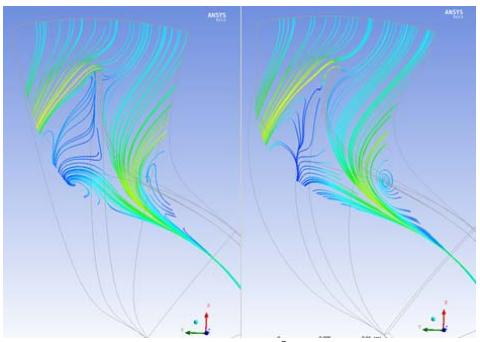

Baseline Radial Rotor 25^0 Back Swept Rotor

(g) Streamline Distribution at 75% Span

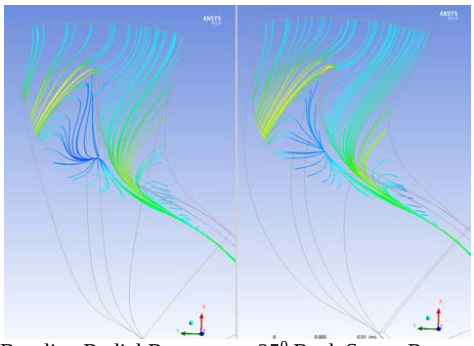

Baseline Radial Rotor 25^0 Back Swept Rotor

(h) Streamline Distribution at 87.5% Span

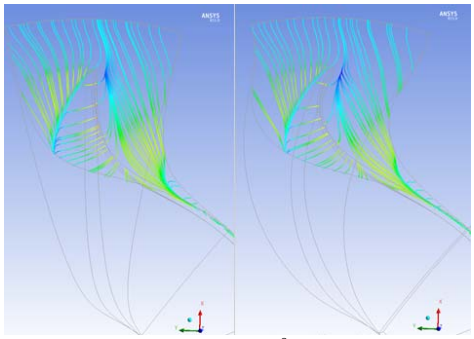

Baseline Radial Rotor 25^0 Back Swept Rotor

(i) Streamline Distribution at 99% Span

Fig. 6. Spanwise Distribution.

On the suction side of radial blade, the zone of recirculation at inlet is seem to increase in size while moving from 12.5% to 37.5% of span, as shown in fig. 6(b) to 6(d). The recirculation on the suction side at inlet to the 25° back swept rotor has also increased, although much smaller in size, protruding further into the blade passage.

At 50% span, on suction side at inlet of both rotors, the recirculation observed beings to diminish gradually in size and strength, resulting a less flow reversal as shown in Fig.6 (e). Here, more of the blade passage is occupy by high velocity flow. A further reduction in zone of recirculation is observed between 62.5% to 75% span. There is less recirculation zone present on the 25^o back swept rotor. This is shown in fig. 6(f) and (g).At 87.5% span, the 25° back swept rotor experiences little less flow reversal then the base line rotor. On the suction side of both rotors, point of separation if present on both rotors at same location, as shown in fig.6(h).Flow patterns for the baseline radial and 25° back swept rotors are almost identical at 99% span, as shown in fig.6(i) as this plot lies within the tip clearance region.

The plots of secondary flow features are shown in figs. 7 (a) to (i). The pressure side of the blade on the left and the suction side of the blade on the right. The direction of rotation is left to right. The hub is at bottom and shroud is at top.

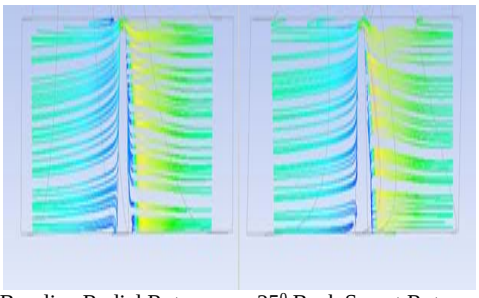

Baseline Radial Rotor 25^0 Back Swept Rotor
(a) Streamline Distribution at LE

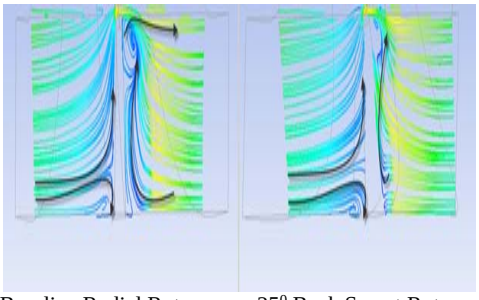

Baseline Radial Rotor 25^0 Back Swept Rotor
(b) Streamline Distribution at 12.5% Chord

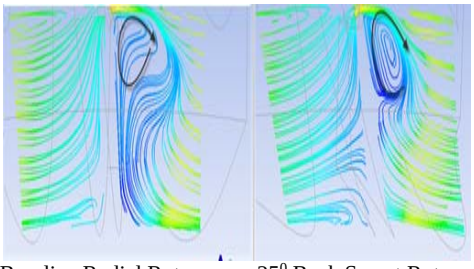

Baseline Radial Rotor 25^0 Back Swept Rotor
(c) Streamline Distribution at 25% Chord

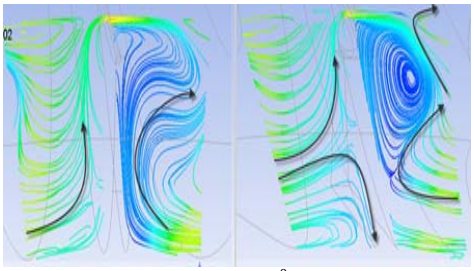

Baseline Radial Rotor 25^0 Back Swept Rotor
(d) Streamline Distribution at 37.5% Chord

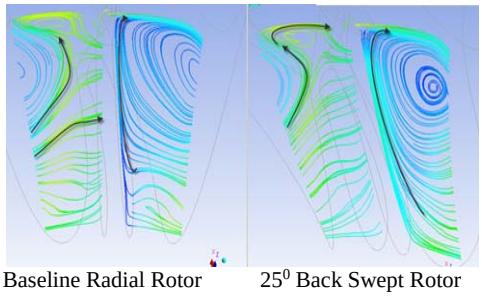

Baseline Radial Rotor 25^0 Back Swept Rotor
(e) Streamline Distribution at 50% Chord

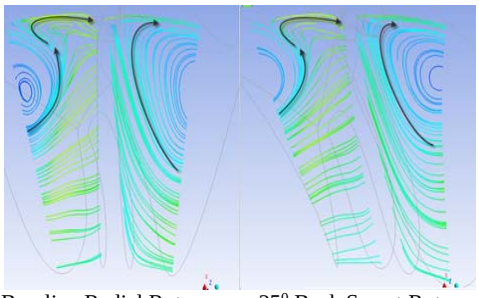

Baseline Radial Rotor 25^0 Back Swept Rotor
(f) Streamline Distribution at 62.5% Chord

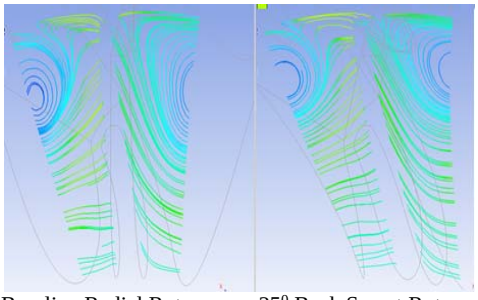

Baseline Radial Rotor 25^0 Back Swept Rotor
(g) Streamline Distribution at 75% Chord

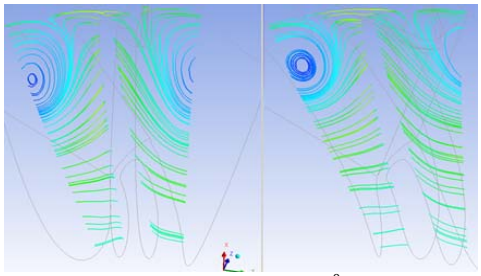

(a) Baseline Radial Rotor (b) 25^0 Back Swept Rotor
(h) Streamline Distribution at 87.5% Chord

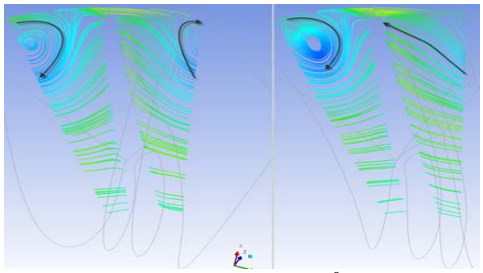

(a) Baseline Radial Rotor (b) 25^0 Back Swept Rotor
(i) Streamline Distribution at TE

Fig. 7. Streamwise Distribution.

The flow is entering in tangential direction, on a just upstream of leading edge as shown in Fig.7 (a). This is because of positive incidence at low velocity ratio. The flow direction from tangential to axial change due to relative shroud wall velocity. The significant reduction in velocity is observed as the flow meets the pressure side of the blade.

At 12.5% of chord, the flow is deviate from

tangential direction as shown in Fig.7 (b). This flow is now traveling along pressure surface. Here almost 75% of flow is turn and travel towards the hub whereas remaining 25% travel towards shroud, which contribute to blade tip leakage. For the backswept rotor, 20% of the flow contribution towards blade tip leakage. On the suction side still majority of flow travels in tangential direction which results a strong positive incidence at inlet. At shroud, small zone of recirculation is present which produce primary zone of recirculation near shroud surface. This zone of recirculation presents in both rotors but the strength of recirculation zone is less in back swept blade.

Now this zone of recirculation is more dominating and converted in to a leading edge vortex as it moves from 12.5% to 25% chord. A leading edge vortex consumes much more of suction side of the blade passage in radial rotor then back swept rotor as shown in Fig.7(c). The couple of tangential flow and flow from hub to shroud causes the tip leakage flow travelling away from suction surface which leads to the tip leakage flow spiraling in a clockwise direction as shown in Fig.7(c).

At 37.5% chord, the leading edge vortex is still dominant flow and continues to have a larger presence within the blade passage of the radial rotor then back swept rotor as shown in Fig. 7 (d). The center of the leading edge vortex is now move towards the hub surface and taking the shortest path through the rotor in a meridional direction.

There is no tip leakage flow on either the radial and back swept rotor at 50% chord as shown in Fig. 7 (e). There is a significant reduction in leading edge vortex between 37.5%to 50% chord. Here the magnitude of leading edge vortex is diminish due to the relative motion of shroud wall which is opposite in the direction and the mass moment of flow on the suction side of both rotor is seen to travel along the hub to shroud direction.

Figures 7 (f) to (h) shows the identical secondary flow features in both rotors. The leading edge vortex is seen to move further from suction surface due to increasing blade swept angle in blade to blade direction.

From Fig.7 (f) and (g), i.e.at 62.5 and 75% chord, the center of leading edge vortex is moving from suction surface to pressure surface and take the positioned slightly closer to pressure surface and remains on the same position till the trailing edge, as shown in Fig.7(h) and (i).

4. COMPARISON OF 1D ANALYSIS WITH 3D CFD ANALYSIS

Figure8 shows the total to static efficiency of radial turbine and back swept blade vs. velocity ratio by 1D approach and 3D CFD simulation. In Fig.30 it is observed that the efficiency of back swept turbine is 4.61% higher than the base line rotor for 1D and 3D simulation up to velocity ration 0f 0.471 than it gradually decrease. After velocity ratio 0.566 the efficiency by numerical simulation decrease drastically that is because of secondary flow losses occurring in blade passage but it did not happen with 1D analysis as it is difficult to predict actual losses in spanwise direction. After velocity ratio 0.613 the numerical simulation is showing domain overflow error and does not converge.

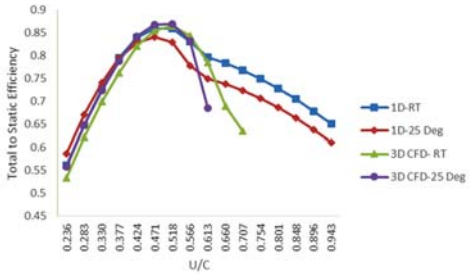

Fig. 8. Total to Static Efficiency vs. Velocity Ratio (Inlet Pressure 1.8 bar).

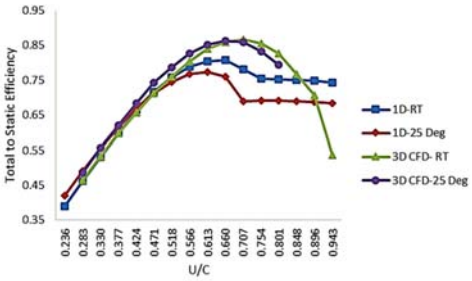

Fig. 9. Total to Static Efficiency vs. Velocity Ratio (Inlet Pressure 2.8 bar).

Figure 9 shows the total to static efficiency of radial turbine and back swept blade vs. velocity ratio by 1D approach and 3D CFD simulation for design condition. In Fig.9 it is observed that the efficiency of back swept turbine is higher than the base line rotor for 1D up to velocity ratio of 0.471 and 3D simulation up to velocity ratio of 0.707(design point) than it gradually decrease. After velocity ratio of 0.707 the efficiency by numerical simulation decreases drastically that is because of secondary flow losses occurring in blade passage but it did not happen with 1D analysis as it is difficult to predict actual losses in spanwise direction. Liam Barr *et al.* (2009) did the numerical analysis on 86 mm radial and back swept turbine and suggested off-design performance gains of 2%. They shows that experimental efficiency of the baseline rotor was seen to lie within a band of4.2% to 4.9% above that predicted numerically.

5. CONCLUSION

Torque available would be more, particularly at lower than optimum values of velocity ratio due to increase in turbine efficiency. A one dimensional analysis suggested that at lower velocity ratio the 25° back swept rotor experienced higher efficiency compared to base line rotor. For example at design pressure and at 40% of design speed back swept turbine gives 8.19% higher efficiency. The trends

predicted from one dimensional analysis also mirroring the three dimensional numerical analysis. Three dimensional numerical analysis shows that 25° back swept rotor offers a considerable elevated efficiency while operating at lower than optimum velocity ratio. The efficiency showed improvements in order of 4.61% at *U/C* = 0.471atinlet pressure of 1.8 bar using the backswept rotor. An increase in mass flow rate through rotor passage is seen due to the reduction in losses offered from 25° back swept rotor. The efficiency of 25° back swept rotor seems drop below the predicted by the radial turbine rotor at design speed (U/C=0.707), however, the small drop in efficiency exhibit at higher velocity ratio are more significant by the large gains in efficiency offered at lower velocity ratio.

REFERENCES

ANSYS Inc. (2009). Ansys CFX14.0 User's Guide. Canonsburg, PA 15317.

AxSTREAM (2014). AxSTREAM User's Guide and Help Manual.

Barr, L., S. W. Spence and P. Eynon (2008). Improved Performance of a Radial Turbine Through the Implimentation of Back Swept Blading.*Proc. Of Turbo Expo*, GT 2008-50064.

Hakeem, I. (1995). *Steady and unsteady Performance of Mixed flow turbines for Automative Turbochargers*. Imperial College of Science, Technology and Medicine, London, England.

Jason, W., S. Spence, J. Ehrhard and D. Thornhill. (2011). An Investigation Into Improving Off-Design Performance in a Turbocharger Turbine utilizing Non-Radial Blading. *Proceedings of ASME Turbo Expo* Vancouver, British Columbia, Canada.

Lee, K. S., K. Y. Kim and A. Samad (2008). Design optimization of low speed axial flow fan blade with three-dimensional RANS analysis. *Journal of mechanical science and technology 1864-1869.*

Liam, B., S. Spence and D. Thornhill (2009). A numerical and experimental performance comparison of an 86 mm radial and back swept turbine. *Proceedings of ASME Turbo Expo.* Orlando, Florida, USA.

Meitner, P. L. and Glassman A. J. (1983) Computer code for off-design performance analysis of Radial Inflow Turbine with Rotor Blade Sweep. *Nasa Technical Paper, Report 2199.*

Menter, F. R., M. Kuntz and R. Langtry (2003). Ten years of industrial experience with the SST turbulence model. *Turbulence, heat and mass transfer*. 625–632.

Menter, F. R., R. Langtry and T. Hansen. (2004) CFD simulation of turbomachinery, validation and modeling. *European Congress on Computational Methods in Applied Sciences and Engineering*, ECCOMAS.

Mulloy, J. M. and H. G. Weber (2001). Radial Inflow Turbine Impeller for Improved Off-Design Performance. *ASME Proc. of 27th International Gas Turbine Conference, New York, USA, 82-GT101.*

Palfreyman, D. and R. Martinez-Botas (2002). Numerical Study of the Internal Flow Field Charecteristics in Mixed Flow Turbines. *Proc of ASME Turbo Expo*, GT 2002-30372.

Pecnik, R., J. A. S. Witteveen and G. Iaccarino (2011). Uncertainty quantification for laminar-turbulent transition prediction in RANS turbomachinery applications. *49th AIAA Aerospace Sciences Meeting including the New Horizons Forum and Aerospace Exposition*.

Simpson, A. T., S. W. T. Spence and J. K. Watterson (2009). A Comparison of the Flow Structures and Losses Within Vaned and Vaneless Stators for Radial Turbines. *Journal of Turbomachinery* 131.

Versteeg, H. K. and W. Malalasekera (2007). *An introduction to computational fluid dynamics: the finite volume method. Prentice Hall.*

Whitfield, A. and N. C. Baines (1990). Design of radial Turbomachines. *Longman Scientific and Technical.*